Time-Resolved Electrochromism Associated with the Formation of Quinone Anions in the *Rhodobacter sphaeroides* R26 Reaction Center[†]

David M. Tiede,* Johana Vázquez,[‡] José Córdova,[§] and Palma Ann Marone

Chemistry Division D-200, Argonne National Laboratory, Argonne, Illinois 60439

Received March 11, 1996; Revised Manuscript Received June 4, 1996[⊗]

ABSTRACT: The bacterial photosynthetic reaction center contains bacteriochlorophyll (Bchl) and bacteriopheophytin (Bph) cofactors that provide natural probes of electrostatic fields within this protein. We have examined the electrochromic responses of these cofactors, resolved during the lifetimes of the quinone anion states, $P^+Q_A^-Q_B$ and $P^+Q_AQ_B^-$, and measured as a function of temperature. These measurements provide information on the time-dependent variation in electrostatic field strength on the Bchl and Bph cofactors. Measurements in the near-infrared absorbance bands have revealed the following. First, the $Q_A^-Q_B \rightarrow Q_AQ_B^-$ electron transfer rate is found to be heterogeneous, consisting of at least two distinct kinetic components. At room temperature, we find a previously unresolved fast kinetic component with a reaction time of 25−40 μs, depending upon the preparation, that accounts for approximately 25% of the total reaction yield. The major component was identified with a reaction time of 210−240 μs. Below −20 °C, $Q_A^-Q_B \rightarrow Q_AQ_B^-$ electron transfer shows distributed kinetics. The temperature-dependent conversion from biphasic to distributed kinetics suggests that there is a thermal averaging of conformational substates around two reaction center configurations. Interestingly, direct excitation of the Bph with 532 nm light at low temperatures appears to alter the electron transfer kinetics, possibly by inducing a change in the distribution of conformational states. The reaction kinetics were found to be sensitive to the addition of ethylene glycol, which is likely to reflect an osmolarity effect. Second, time-dependent absorption changes of the Bchl and Bph cofactors are found to be kinetically decoupled. The rapid responses of the Bph bands are interpreted to reflect electron transfer, while the slower responses of the Bchl are interpreted to reflect slower relaxation events, possibly including proton uptake. Finally, we find that the electrochromic response and $Q_A^-Q_B \rightarrow Q_AQ_B^-$ electron transfer to be sensitive to the preparative state of the reaction center, reflecting differences in quinone binding for reaction centers in different states of purification.

Photosynthetic reaction centers are integral membrane proteins that serve as useful models for biological electron and proton transfers. Bacterial reaction centers contain two sets of bacteriochlorophyll (Bchl), bacteriopheophytin (Bph), and quinone (Q) cofactors arranged symmetrically with respect to a bacteriochlorophyll dimer (P) (Feher et al., 1989; Gunner, 1991; Okamura & Feher, 1992; Shinkarev & Wraight, 1993). Light initiates electron transfer reaction from P to one set of cofactors, terminating in the sequential electron transfer between quinone cofactors, Q_A and Q_B:

$$PQ_AQ_B + h\nu \rightleftarrows P^+Q_A^-Q_B \rightleftarrows P^+Q_AQ_B^-$$

In *Rhodobacter sphaeroides*, Q_A and Q_B are both ubiquinone$_{10}$ molecules, but crystal structures show that the protein environments of the two quinones are significantly different (Allen et al., 1988; Arnoux et al., 1989; El-Kabbani et al., 1991; Ermler et al., 1994). The two quinones differ in hydrogen-bonding contacts with the protein, and the Q_B site is more polar than the Q_A site. As a result of these structural differences, the two quinones are seen to have different redox, spectroscopic, and functional properties (Feher et al., 1989; Gunner, 1991; Okamura & Feher, 1992; Shinkarev & Wraight, 1993). Q_A functions as a fixed, one-electron acceptor. Reoxidation of Q_A^- by electron tranfer to Q_B is required in order to ellicit further turnovers of the reaction center. In contrast, Q_B functions as a two-electron, two-proton acceptor that leaves the reaction center following reduction to the dihydroquionone form (Feher et al., 1989; Gunner, 1991; Okamura & Feher, 1992; Shinkarev & Wraight, 1993).

Relaxation events, such as conformational changes or proton transfer, can be expected to accompany the sudden generation of charge in the reaction center. Relaxation events associated with the formation of the quinone anion states are of particular importance because of the physiologically necessary proton uptake that is coupled to these reactions. Stoichiometries of proton uptake for Q_A^- and Q_B^- differ, and they depend strongly upon pH (Feher et al., 1989; Gunner, 1991; Okamura & Feher, 1992; Shinkarev & Wraight, 1993). Spectroscopic data show that the quinone anions themselves are not protonated but that the proton uptake is associated with the protonation of amino acid residues (Feher et al., 1989; Gunner, 1991; Okamura &

[†] This work was supported by the U.S. Department of Energy, Office of Basic Energy Sciences, Division of Chemical Sciences, Photochemical and Radiation Sciences Program, under Contract W-31-109-Eng-38. J.V. and J.C. were partially supported by the Argonne National Laboratory Educational Programs Division, Undergraduate Research Participation and Faculty Research Participation Programs, respectively.

* Corresponding author: David M. Tiede, Chemistry Division D-200, Argonne National Laboratory, Argonne, IL 60439. Phone: 708-252-3539. Fax: 708-252-9289. E-Mail: tiede@anlchm.chm.anl.gov.

[‡] Present address: Department of Plant Biology, University of Illinois, 190 EMRL, 1201 W. Gregory Drive, Urbana, IL 61801.

[§] Present address: Department of Chemistry, P.O. Box 12383, Universidad del Sagrado Corazon, San Juan, Puerto Rico 00914-0383.

[⊗] Abstract published in *Advance ACS Abstracts,* August 1, 1996.

S0006-2960(96)00590-9 CCC: $12.00

Feher, 1992; Shinkarev & Wraight, 1993). Dielectric continuum calculations find that the proton uptake stoichiometries and experimentally observed protonation of amino acid residues can be qualitatively explained by a model in which the quinone anions are electrostatically coupled to networks of interacting, ionizable amino acid side chains (Beroza et al., 1991, 1995; Gunner & Honig, 1991). The generation of charge on the quinone is calculated to cause p*K* shifts distributed throughout the network of interacting residues. In this mechanism, the proton uptake compensates for the formation of negative charge on the quinones. However, quantitative disagreements between calculation and experiment have led to the suggestion that other factors such as conformational relaxation also need to be taken into account (Beroza et al., 1995).

The reaction center cofactors provide natural probes of electrostatic fields inside the reaction center (Hanson et al., 1987; Tiede & Hanson, 1992; Steffen et al., 1994). The electrochromism associated with quinone anion formation potentially offers a valuable means to monitor internal movements of protons and other counterions in response to the formation of the quinone anion states. Spectra of the optical absorbance changes induced in the Bchl and Bph bands by the formation of Q_A^- and Q_B^- in trapped PQ^- states have been described (Shopes & Wraight, 1985; Vermeglio & Clayton, 1977). The Q_A^- and Q_B^- spectra in the near-infrared region differ in two characteristic ways. First, the zero crossing point of the Bph Q_y band shift associated with the Q_A^- state is displaced to the red compared to that observed for the Q_B^- state. This can be understood from the crystal structures (Allen et al., 1988; El-Kabbani et al., 1991; Ermler et al., 1994). Q_A is seen to be positioned closer to the Bph whose absorption maximum has been identified to be red-shifted compared with that of the inactive Bph (Bylina et al., 1988), which is closer to that of Q_B. Second, the magnitudes of the Bchl and Bph absorption changes induced by Q_A^- formation are greater than those induced by Q_B^- formation. The quenching of Q_B^- electrochromism with respect to that for Q_A^- could arise either from a higher local dielectric surrounding Q_B^- or from the movement of a proton or other counterion into the vicinity of the Q_B^-. The spectra reported for the Q_A^- and Q_B^- states have been recorded long after proton uptake occurs, and hence, these spectra can be taken to represent fully relaxed states.

Analysis of the time-dependent electrochromism associated with the $Q_A^-Q_B \rightarrow Q_AQ_B^-$ electron transfer is important since the reaction center cofactor electrochromism provides information on both electron transfer and electrostatic relaxation events. The time-dependent responses of the cofactor electrochromism to quinone anion formation have been only partially characterized. The electrochromic shifts in the Bph band region during the $Q_A^-Q_B \rightarrow Q_AQ_B^-$ electron transfer have been measured by single-wavelength transients in isolated *Rb. sphaeroides* reaction centers (Kleinfeld et al., 1984a; Mancino et al., 1984; Shopes & Wraight, 1985; Vermeglio & Clayton, 1977). Reaction rates are typically reported to be in the 100−200 μs^{-1} range. However, references have been made to the possibility of more complex kinetics in Bph absorption transients in *Rb. sphaeroides* (Takahashi & Wraight, 1992) and in double-flash experiments that probe the rate of $Q_A^-Q_B \rightarrow Q_AQ_B^-$ electron transfer in *Rhodopseudomonas viridis* (Carithers & Parson, 1975; Leibl & Breton, 1991). Besides the electron transfer event, preliminary measurements in *Rhodobacter capsulatus* chromatophores suggest that the time-resolved electrochromism associated with the $P^+Q_A^-$ and $P^+Q_B^-$ states may also reflect secondary charge movement or relaxation events (Tiede & Hanson, 1992). Evidence for conformational relaxation in isolated reaction centers following quinone anion formation has also been suggested from other experiments. Measurements of capacitative charge movement with reaction centers imbedded in supported planar bilayers have found evidence for a 200 μs^{-1} conformational change that is possibly the rate-limiting step for electron transfer (Brzezinski et al., 1992). Transient IR measurements have also found evidence for rapid changes in the vibrational spectrum due to electron transfer, along with slower kinetics reflecting relaxation events (Hienerwadel et al., 1992, 1995). Biphasic $P^+Q_A^-$ recombination kinetics have suggested the existence of at least two reaction center configurations (Franzen et al., 1990; Kleinfeld et al., 1984b; Parot et al., 1987; Sebban & Wraight, 1989), and the ability to use light to freeze reaction centers in configurations with altered electron transfer kinetics (Kleinfeld et al., 1984b) has indicated the existence of conformational relaxation during the lifetimes of the P^+Q^- states. An understanding of the relationship between protein relaxation and proton uptake in reaction centers will require a more detailed characterization of how the relaxation events are linked to quinone anion charge stabilization.

In this paper, we present a detailed characterization of the electrochromic response of the reaction center cofactors, resolved during the lifetimes of the $P^+Q_A^-Q_B$ and $P^+Q_AQ_B^-$ states and measured as a function of temperature. These measurements provide information on the time-dependent variation in electrostatic field strength on the Bchl and Bph cofactors. These experiments resolve the following features about the electrochromic response. First, the $Q_A^-Q_B \rightarrow Q_AQ_B^-$ electron transfer rate is found to be heterogeneous, consisting of at least two distinct kinetic components. The temperature-dependent changes in the kinetics suggest that the $Q_A^-Q_B \rightarrow Q_AQ_B^-$ electron transfer is likely to reflect a thermal averaging of conformational substates, similar to that seen for reaction dynamics in other proteins (Frauenfelder & Wolynes, 1994; Hagen et al., 1995). Second, time-dependent changes in the electrochromism spectra show that the absorbance changes of the Bchl and Bph cofactors are not kinetically coupled. We interpret the rapid responses of the Bph band to reflect electron transfer, while the slower Bchl responses appear to reflect slower relaxation events that possibly include proton uptake. Finally, we find that the electrochromic response and $Q_A^-Q_B \rightarrow Q_AQ_B^-$ electron transfer to be sensitive to the preparative state of the reaction center, reflecting differences in quinone binding for reaction centers in different states of purification.

MATERIALS AND METHODS

Preparation of Reaction Centers. Reaction centers were prepared from *Rb. sphaeroides* R26 chromatophores following procedures adapted from Wraight (1979). Chromatophores were incubated for 1 h in 0.1 M NaCl and 10 mM Tris at pH 7.8 with 0.6% lauryl dimethylamine-*N*-oxide (LDAO). The supernatant from a 50 000 rpm centrifugation was brought to 1% LDAO, and $(NH_4)_2SO_4$ was added to 0.3 g/mL. The mixture was centrifuged for 10 min at 10 000 rpm. The resulting floatate was recovered and dissolved in

0.15% LDAO and 10 mM Tris at pH 7.8. $(NH_4)_2SO_4$ was progressively added in the 0.1−0.15 g/mL range, and the sample was centrifuged, up to the point where reaction centers appeared in the precipitate. The bulk of the reaction centers were then recovered by addition of 0.25 g/mL $(NH_4)_2SO_4$ and centrifugation. The floatate was dissolved in 0.1% LDAO and 10 mM Tris at pH 7.8 and loaded onto a sucrose gradient (20 to 50% w/v) with 10 mM Tris at pH 7.8 and either 0.1% LDAO or 0.8% *n*-octyl β-D-glucoside (OG) and centrifuged overnight at 50 000 rpm. The reaction center band was collected and dialyzed against 10 mM Tris at pH 7.8 and either 0.1% LDAO or 0.8% OG. The resulting, partially purified reaction centers were found to contain the full complement of functional Q_B, as determined by P^+Q^- recombination kinetics, and are referred to as native Q_B reaction centers. The 280 nm/802 nm ratio varied from 1.4 to 2.5, depending upon the efficiencies of the $(NH_4)_2SO_4$ fractionation and sucrose gradient.

Purified reaction centers were prepared by dialyzing the native Q_B reaction centers against 0.06% LDAO and 10 mM Tris at pH 7.8 overnight at 4 °C and then loading onto a Sephadex DEAE column. The reaction centers were washed extensively with 0.06% LDAO, 60 mM NaCl, and 10 mM Tris at pH 7.8 and eluted with 280 mM NaCl, 10 mM Tris at pH 7.8, and either 0.06% LDAO or 0.8% OG. The purified reaction center band had 280 nm/802 nm absorbance ratios in the 1.2−1.3 range. Reaction centers were stored frozen at −80 °C and dialyzed prior to use. Light-induced charge recombination kinetics suggested that the Q_B site occupancy was 20−30%. Q_B was reconstituted by adding quinone from a stock solution containing 2 mM ubiquinone$_{10}$ (Sigma) with either 1% LDAO or 10% Triton that had been heated to 50 °C for approximately 5 min. The resulting solutions contained 10−15 μM reaction centers and 100 μM quinone.

Measurement of Optical Absorption Changes Associated with the $Q_A^-Q_B \rightarrow Q_AQ_B^-$ Electron Transfer. Optical absorption changes associated with quinone anions in transient P^+Q^- states were identified by recording transient spectra as a function of time between a 30 ns (full width at half-height) laser excitation pulse and a weak 0.65 μs (full width at half-height) xenon probe pulse, using a 1024-element, single-diode array, multiwavelength detector (EG&G). Transient absorbance spectra, $A(\lambda,t) = \log[I_o(\lambda)/I(\lambda,t)]$, were calculated by recording transmitted probe light before, $I_o(\lambda)$, laser excitation and with a variable time delay, t, after laser excitation, $I(\lambda,t)$. Both $I_o(\lambda)$ and $I(\lambda,t)$ were corrected for pixel-dependent charge accumulation in the dark, and $I(\lambda,t)$ was corrected for a fluorescence artifact recorded with laser excitation in the absence of a probe pulse. The laser pulse was either the frequency-doubled, 532 nm output from a Molectron Nd:YAG laser or the 614 nm emission from a 532 nm Nd:YAG pumped Rhodamine 640 (Exciton) dye laser. Laser intensities were adjusted in the 2−5 mJ/cm^2 range to provide 60−80% saturation of reaction center photochemistry. The xenon flash light was focused upon a 3 mm diameter fiber optic bundle (Oriel) and passed through a long wave pass glass filter that transmitted light above 580 nm (Corion). The actinic properties of the xenon probe beam were determined by measurement of the amplitudes of absorbance changes induced by successive xenon pulses without laser excitation. The absorbance changes induced by successive xenon pulses were less than 1% of those detected following laser excitation.

The sample cuvette consisted of a flow cell constructed from a 3 mm stainless steel spacer with plexiglass windows. For temperature control, the sample cuvette was placed in a nitrogen-purged dewar. The temperature was approximately set by regulating the nitrogen flow through either a dry ice or liquid nitrogen bath. The stainless steel spacer served as a cold finger whose temperature was regulated within ±1 °C by a thermoelectric controller (Alpha Omega). The spectra measured for a single delay time are the average of five to ten acquisitions. Experiments that recorded absorbance spectra as a function of time across the 1 μs to 1 s range typically involved measurement of 30−100 spectra. A computer-controlled peristaltic pump was used to provide a fresh, dark-adapted sample just prior to each laser flash. The flash repetition rate and sample reservoir volume were adjusted to provide at least 3 min of dark time between laser exposures for individual sample volume elements.

The light pulse from the xenon flash lamp has an asymmetric shape. Flash profiles were measured in the reaction cofactor absorption band regions using 760, 800, and 850 nm interference filters (12 nm FWHM). The flash profiles in these regions were equivalent. The peak intensity is reached in 0.4 μs and then shows a complex decay that could be fit as a biexponential, with 90% of the intensity decaying with a 0.48 μs time constant and 10% decaying with a 3.4 μs time constant. The time-resolved absorbance transients are a convolution of the probe pulse profile, $Xe(t)$, and the optical response of the reaction centers, $S(\lambda,t)$. The rise of the xenon pulse is slow compared to the primary reactions. As a result, the earliest transient spectrum measured by the xenon probe, even with a zero time delay between pump and probe pulses, is that of the initial $P^+Q_A^-$ state. Subsequent spectra measure absorption changes associated with time evolution of the P^+Q^- states. These time-dependent changes were identified from transient difference spectra, $\Delta A(\lambda,t) = A(\lambda,t) - A(\lambda,0)$, calculated by subtracting the transient spectrum measured with a zero time delay from subsequent spectra. The difference spectrum can be written in terms of the convolution of the probe pulse with the reaction center optical response (Demas, 1983; Tang & Norris, 1988).

$$\Delta A(\lambda,t) = \sum_{\delta}[Xe(\delta)S(\lambda,t+\delta) - Xe(\delta)S(\lambda,\delta)] \quad (1)$$

The transient difference spectra identify the absorption changes occurring after the formation of the $P^+Q_A^-$ state. The difference absorption transients, $A(,t) - A(\lambda,0\ \mu s)$, were fit using eq 1 and with $S(\lambda,t)$ described as a sum exponential components:

$$S(\lambda,t) = \sum_{k} B(\lambda,k)[1 - e^{-t/\tau(\lambda,k)}] \quad (2)$$

where the number of components, k, used to fit the data was 1−3. Note that the amplitudes of the exponential components, $B(\lambda,k)$, and their lifetimes, $\tau(\lambda,k)$, were fit independently as a function of wavelength. Curve fittings of difference transients at single wavelengths were done using a Levenberg−Marquardt, nonlinear least squares routine (Press et al., 1992), available in MATHCAD (MathSoft).

The kinetic components determined by this analysis are somewhat dependent upon the shape of the xenon probe

pulse. For example, if the white light output of the lamp is measured without the interference filters described above, a different pulse shape is measured. The complex intensity decay can be described as a biexponential with 90% decaying with a 1.5 μs lifetime and 10% decaying with a 15 μs lifetime. If the white light pulse shape is used in the fitting procedure, then the reaction lifetimes are only marginally changed, <10%, from the values reported in this paper. The use of this pulse shape did cause the amplitudes of the fitted components to vary by up to 10% from the values reported below. We believe that the most correct procedure is to use the xenon pulse shape measured in the wavelength regions of the reaction center cofactors, but this comparison does give an estimate of the sensitivity of the fitted kinetic parameters to the probe pulse shape.

Experimentally, the transient difference spectra were obtained by subtracting normalized spectra measured with a zero time delay from those measured with longer delays: $\Delta A(\lambda,t) = A(\lambda,t) - nA(\lambda,0\ \mu s)$. The normalization constant, n, was chosen to match the absorbance decreases of P at 865 nm. This normalization compensated for the loss of P^+ due to charge recombination and for slight shot-to-shot variations in reaction center excitation. The resulting difference spectra eliminated absorbance changes associated with the formation of the initial $P^+Q_A^-$ state and produced difference spectra of the absorbance changes associated with subsequent relaxation and electron transfer events. Finally, all of the difference spectra shown in this paper have been normalized by dividing by the initial absorbance change at 865 nm:

$$\Delta A(\lambda,t) = \Delta A(\lambda,t)/A(865\ \text{nm}, 0\ \mu s) \qquad (3)$$

This normalization removes amplitude variations in these spectra due to experiment-to-experiment differences in reaction center concentration and laser saturation. This normalization also allows the resulting difference spectra reported in this paper recorded with different experimental conditions to be quantitatively compared.

RESULTS

Comparison of Reaction Centers with Native and Reconstituted Q_B. The $Q_A^-Q_B \rightarrow Q_AQ_B^-$ electron transfer and accompanying proton transfers are frequently assayed with purified reaction centers in which the Q_B lost during purification is reconstituted with quinone from detergent solutions (Mancino et al., 1984; Maroti & Wraight, 1988; McPherson et al., 1988; Paddock et al., 1991). The need to reconstitute Q_B in purified reaction centers raises the possibility that the quinone extraction and reconstitution might cause structural variation in the Q_B binding domain. We have also examined the optical absorption changes associated with the $Q_A^-Q_B \rightarrow Q_AQ_B^-$ reaction with partially purified reaction centers that contain the full complement of native quinone in the Q_B site. These native Q_B-containing reaction centers allow the $Q_A^-Q_B \rightarrow Q_AQ_B^-$ electron transfer to be characterized in the absence of exogenous quinone additions, and potentially with a more intact Q_B binding site. Differences in $Q_A^-Q_B \rightarrow Q_AQ_B^-$ electron transfer were found between reaction centers that contained native Q_B and those that contained reconstituted Q_B. One noticeable difference was in the yield of $P^+Q_B^-$ generated by illumination at low temperatures.

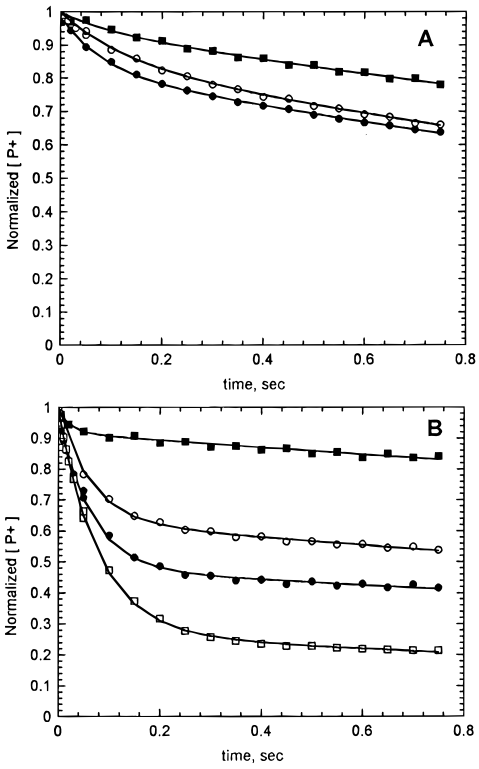

FIGURE 1: Yield of $P^+Q_B^-$ assayed by P^+ recombination kinetics measured at 860 nm in different reaction center preparations. The data in Part A were recorded with room-temperature samples in 0.8% OG and 10 mM Tris at pH 7.8. The squares mark data for native Q_B reaction centers. The open and filled circles mark data for Q_B reconstituted reaction centers, using quinone stock solutions in 1% LDAO and 10% Triton X-100, respectively. The reconstitution procedures are described in Materials and Methods. Part B shows recombination kinetics measured for samples at −20 °C in 50% ethylene glycol, 0.8% LDAO, and 10 mM Tris at pH 7.8. The filled squares mark data from native Q_B reaction centers, the open circles LDAO Q_B reconstituted reaction centers, the closed circles Triton X-100 Q_B reconstituted reaction centers, and the open squares Q_B-depleted reaction centers. The solid lines are fits with biexponential decays.

Figure 1 compares the yield of $P^+Q_B^-$ in native and reconstituted Q_B reaction centers at room temperature and at −20 °C. $P^+Q_B^-$ yield was assayed by fitting P^+ decay as a sum of two exponentials. Recombination from $P^+Q_A^-$ occurs with a reaction time that is approximately 10-fold shorter than that of $P^+Q_B^-$ (Feher et al., 1989; Gunner, 1991; Okamura & Feher, 1992; Paddock et al., 1991). At room temperature, native and reconstituted Q_B reaction centers show similar P^+ decay characteristics. For native Q_B reaction centers in 50% ethylene glycol, the P^+ decay followed a time course in which 95% of the decay occurred with a lifetime of approximately 3 s, attributable to decay from $P^+Q_B^-$. The $P^+Q_B^-$ decay time is lengthened by ethylene glycol in both native and reconstituted Q_B reaction centers as described below. Similar results were also found by Larson and Wraight (1995). The remaining 5% was fit with a decay lifetime of 0.1 s, attributable to decay from $P^+Q_A^-$. With Q_B reconstituted reaction centers, $P^+Q_B^-$ recombination exhibited a similar, approximately 3 s decay time, but the yield was in the 80−85% range.

Differences in the yield of $P^+Q_B^-$ were more evident at lower temperatures as shown in Figure 1B. For example, at −20 °C, $P^+Q_B^-$ yields were found in the 80−95% range for native Q_B reaction centers, while significantly lower

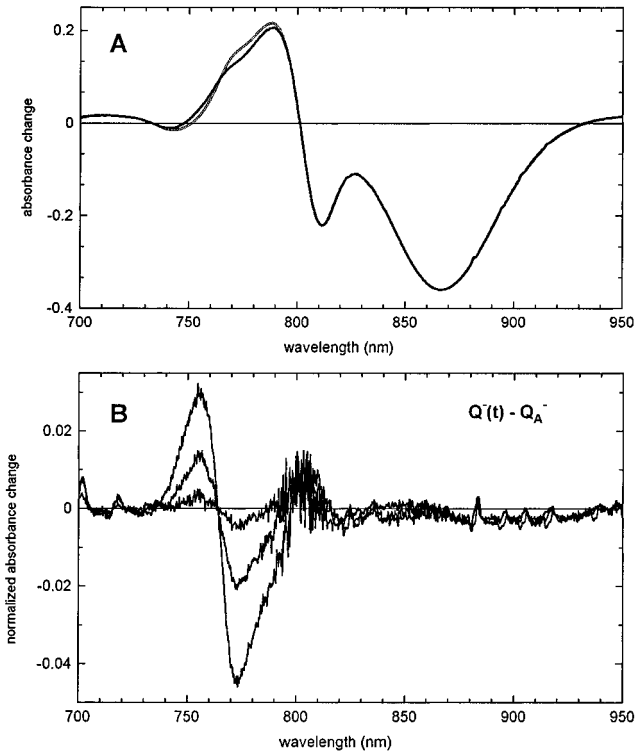

FIGURE 2: Part A shows transient $(P^+Q^-)_t$ spectra for reconstituted Q_B reaction centers at room temperature. The dotted and solid lines mark spectra measured 0 μs and 50 ms following 614 nm laser excitation. The reaction centers were suspended in 0.8% OG and 10 mM Tris at pH 7.8. Part B shows $Q^-(t) - Q_A^-(0\ \mu s)$ difference spectra, calculated from transient P^+Q^- spectra described in part A and recorded with delay times of 10 μs, 100 μs, and 50 ms. Q_B was reconstituted from LDAO stock solutions.

yields in the 45−60% range were found for reaction center samples with Q_B reconstituted from Triton X-100 and LDAO solutions, respectively. These measurements are likely to underestimate the loss in low-temperature $P^+Q_B^-$ yield in reconstituted reaction centers, since the Q_B-depleted reaction centers showed approximately 27% $P^+Q_B^-$ activity at both 22 and −20 °C before reconstitution, as indicated in Figure 1B. This suggests that a significant fraction of the low-temperature $P^+Q_B^-$ yield in reconstituted reaction centers originates from the residual native Q_B in these preparations. The attenuation of low-temperature $Q_A^-Q_B \rightarrow Q_AQ_B^-$ activity suggests that there is likely to be some perturbation of structure in the quinone binding domains in reconstituted reaction centers. The examination of absorption transients described below shows that this loss of low-temperature yield is due to a slower $Q_A^-Q_B \rightarrow Q_AQ_B^-$ electron transfer rate that competes less successfully with $P^+Q_A^-$ recombination at low temperatures.

Absorption Changes Associated with the $Q_A^-Q_B \rightarrow Q_AQ_B^-$ Electron Transfer at Room Temperature. Representative transient spectra, $(P^+Q^-)_t$, are shown in Figure 2A, measured at room temperature with 0 μs and 50 ms time delays, using Q_B reconstituted reaction centers. The two spectra correspond to the initial $P^+Q_A^-$ and final $P^+Q_B^-$ states, respectively. Both spectra are dominated by the absorbance changes associated with P^+. However, the two spectra differ noticeably in the minor inflections seen in the 760 nm region. These changes are indicative of differences in the electrochromic shifts of the Bph cofactors. The magnitude of this feature is larger in the $P^+Q_A^-$ spectrum, and the zero crossing point is shifted further to the red compared to that of the $P^+Q_B^-$ spectrum. These features are consistent with absorption changes measured for quinone anion states PQ_A^- and PQ_B^-, trapped using exogenous electron donors to re-reduce P^+ in the presence and absence of Q_B site inhibitors (Shopes & Wraight, 1985; Vermeglio & Clayton, 1977). The differences between the two spectra in Figure 2 reflect the absorption changes between the $P^+Q_A^-Q_B$ and $P^+Q_AQ_B^-$ redox states. Measurements of single-wavelength absorbance transients at 750 nm have been used to measure the kinetics of $Q_A^-Q_B \rightarrow Q_AQ_B^-$ electron transfer (Kleinfeld et al., 1984a; Mancino et al., 1984; Shopes & Wraight, 1985; Vermeglio & Clayton, 1977).

A more detailed description of the absorption changes accompanying the $Q_A^-Q_B \rightarrow Q_AQ_B^-$ electron transfer can be obtained by removing the contribution of P^+ from these spectra. This was done by subtracting a normalized, initial $(P^+Q_A^-)_{0\ \mu s}$ spectrum, measured with zero time between excitation and probe pulses, from $(P^+Q^-)_t$ spectra measured with longer time delays. The electrochromism associated with P^+ can be anticipated to be approximately constant with time, while the electrochromism due to the quinones can be anticipated to change as a result of the $Q_A^-Q_B \rightarrow Q_AQ_B^-$ electron transfer and subsequent relaxation events.

Figure 2B shows difference spectra, $N_0[(P^+Q^-)_t - n_t(P^+Q_A^-)_{0\ \mu s}]$, calculated from the $(P^+Q^-)_t$ spectra for Q_B reconstituted reaction centers at room temperature. The normalization constant, n_t, is used to compensate for slight variations and decay of P^+ in individual $(P^+Q^-)_t$ spectra, and N_0 is used to scale the difference spectra to ΔA(865 nm, 0 μs) = 1. n_t varies for individual $(P^+Q^-)_t$ spectra, but N_0 is constant for the experiment. The difference spectrum obtained with a 50 ms delay time is approximately matched to a difference spectrum calculated from spectra recorded for the two trapped states, PQ_B^- and PQ_A^-, using ferrocene as an electron donor to P^+ in the absence and presence of *o*-phenanthroline (data not shown). This correspondence supports the assumption that the time-dependent absorbance changes associated with P^+ make minor contributions to time evolution in the P^+Q^- spectra. This assumption was also tested below by comparing the time-dependent changes in $P^+Q_A^-$ spectra under conditions where electron transfer to Q_B occurs and where it is blocked by inhibitor. Two sets of four sharp lines are noticeable in some of the spectra in the 820−840 nm and 880−920 nm wavelength regions. These lines arise from slight pulse-to-pulse variations in the intensities of the xenon lines in the probe light.

The difference spectra shown in Figure 2B appear as slightly asymmetric, derivative band shapes centered near 764 nm due to the Bph absorbance shifts. Smaller, less well-resolved absorption changes are also seen in these spectra near 800 nm. These features are likely to reflect changes in the monomeric Bchl absorptions. Apart from changes in amplitude, there are no noticeable changes in the difference spectra as the $Q_A^-Q_B \rightarrow Q_AQ_B^-$ electron transfer proceeds at room temperature.

The kinetics of the build-in of absorbance changes at single wavelengths are shown in Figure 3, with time plotted on a logarithmic scale. We note that, on this type of plot, first-order, exponential rate processes have sigmoidal shapes. Figure 3 shows transients measured at the difference peak (757 nm) and trough (770 nm). The absorbance decreases at 770 nm are plotted with an inverted sign. The figure also

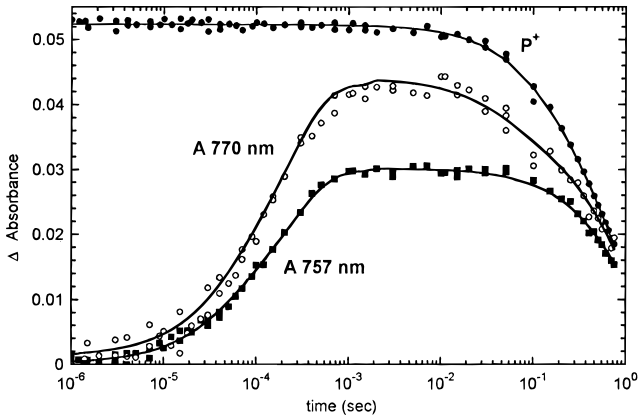

FIGURE 3: Time course for absorbance changes associated with the $Q_A^-Q_B \rightarrow Q_AQ_B^-$ electron transfer in reconstituted Q_B reaction centers at room temperature. Absorbance changes at 757 nm (filled squares) and 770 nm (open circles) were taken from the spectra described in Figure 2. The 770 nm absorption changes are plotted with an inverted sign, and the amplitudes of the 757 and 770 nm absorbance changes are normalized to ΔA(865 nm, 0 μs) = 1. The filled circles mark the extent of P^+ measured by 865 nm bleaching and scaled to fit into the figure. The solid lines are fits described in the text.

shows the extent of P^+, measured by the amplitude of the absorbance decrease at 865 nm. The P^+ data were scaled arbitrarily to fit into the figure. The solid lines in Figure 3 show best fits using the procedures described in Materials and Methods. Fits to the 757 nm data used a biexponential rise, having rise times of 37 ± 17 and 233 ± 50 μs with relative amplitudes of 0.23 and 0.77, respectively. Fits to the transients at 770 nm were similar, having rise times of 41 ± 29 and 239 ± 65 μs with relative amplitudes of 0.25 and 0.75, respectively. Significantly, these experiments find that the electrochromic responses to the $Q_A^-Q_B \rightarrow Q_AQ_B^-$ electron transfer cannot be fit with single-exponential kinetics at room temperature.

The decays of the absorbance transients were also fit with multiple-exponential decays. With our current protocol, decay components with lifetimes approaching 1 s and longer are undersampled, and hence, the current data yield only rough approximations for the lifetimes of these components. The decay of P^+ was monitored by fitting absorbance changes at 865 nm with a biexponential decay. Eighty-two percent of the signal was fit with a 1 s decay time, attributable to recombination from $P^+Q_B^-$, and the remaining 18% was fit with a decay time of 0.1 s, attributable to decay from $P^+Q_A^-$. The decay at 757 nm in this data set was fit with single exponential with a 1.5 s lifetime. In other samples, the 757 nm decay time more nearly matched the slow P^+ decay. The absence of a rapid decay component in the 757 nm data suggests that the absorbance transients at this wavelength do not respond to changes in the Q_A^- or P^+ states but respond only to changes in the Q_B^- state. In contrast, the decay at 770 nm required two components, 85% associated with a decay time of 0.08 s and 15% with a decay time of 1.0 s. These results suggest that the 770 nm transients respond to changes in both the Q_A^- and Q_B^- states. These indications are more clearly supported in measurements made at lower temperatures, and with the addition of Q_B inhibitors.

Difference spectra associated with the $Q_A^-Q_B \rightarrow Q_AQ_B^-$ electron transfer in reaction centers containing native Q_B were found to be generally similar to those measured with

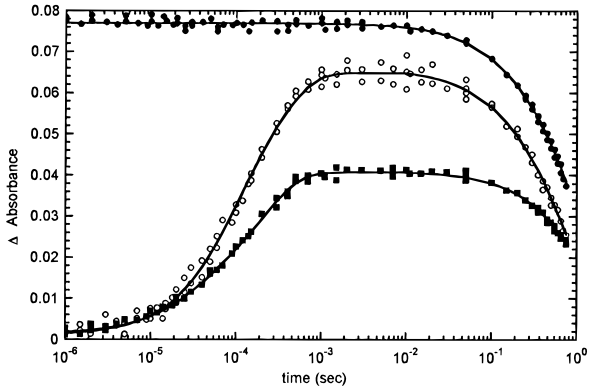

FIGURE 4: Time course for absorbance changes associated with the $Q_A^-Q_B \rightarrow Q_AQ_B^-$ electron transfer in native Q_B reaction centers at room temperature. Absorbance changes at 757 nm (filled squares) and 770 nm (open circles) were taken from the spectra described in Figure 3. The 770 nm absorption changes are plotted with an inverted sign, and the amplitudes of the 757 and 770 nm absorbance changes are normalized to ΔA(865 nm, 0 μs) = 1. The filled circles mark the extent of P^+ measured by 865 nm bleaching and scaled to fit into the figure. The solid lines are fits described in the text.

reconstituted Q_B. Although, these spectra tended to exhibit slightly more prominent absorption shifts of the Bchl cofactors near 800 nm than were seen with reconstituted Q_B preparations (data not shown).

The kinetics of the absorbance changes in native Q_B reaction centers at room temperature were found to differ slightly from those measured in reconstituted Q_B preparations. The kinetics of the absorbance changes at 757 and 770 nm are shown in Figure 4. The rise times of the absorbance changes at 757 nm were found to be slightly faster than those measured with reconstituted Q_B, and differences between kinetics at 757 and 770 nm were seen in the native Q_B preparations that had not been seen with the reconstituted preparations. The absorbance increases at 757 nm in native Q_B reaction centers were fit with a biexponential rise, having lifetimes of 25 ± 8 and 208 ± 17 μs, with relative amplitudes of 0.25 and 0.75, respectively. In contrast, the absorbance changes at 770 nm were fit with lifetimes of 41 ± 25 and 219 ± 33 μs, with relative amplitudes of 0.23 and 0.77, respectively. A key feature to be noted from these results is that the absorbance transients associated with the $Q_A^-Q_B \rightarrow Q_AQ_B^-$ electron transfer in native Q_B reaction centers are complex and cannot be fit by a single, wavelength-independent monotonic rise. This reinforces observations in reconstituted reaction centers and can be more clearly demonstrated with kinetics measured at low temperatures.

Effect of Ethylene Glycol. Reaction centers were suspended in 50% ethylene glycol in order to examine the optical response of the cofactors to the $Q_A^-Q_B \rightarrow Q_AQ_B^-$ electron transfer below 0 °C. Ethylene glycol can be expected to alter the hydration state of the reaction center due to the increased solution osmolarity. Osmotic stress has been shown to modify the reactivity of several enzymes (Colombo et al., 1992; Parsegian et al., 1986; Rand, 1992), and it has been found to slow electron recombination from $P^+Q_B^-$ and to speed the second electron transfer, $Q_A^-Q_B^- \rightarrow Q_AQ_BH_2$, in bacterial reaction centers (Larson & Wraight, 1995). We show here that ethylene glycol also increases the rate for the first electron transfer, $Q_A^-Q_B \rightarrow Q_AQ_B^-$.

Figure 5 shows 757 and 770 nm kinetics for reaction centers in 50% ethylene glycol at room temperature. The

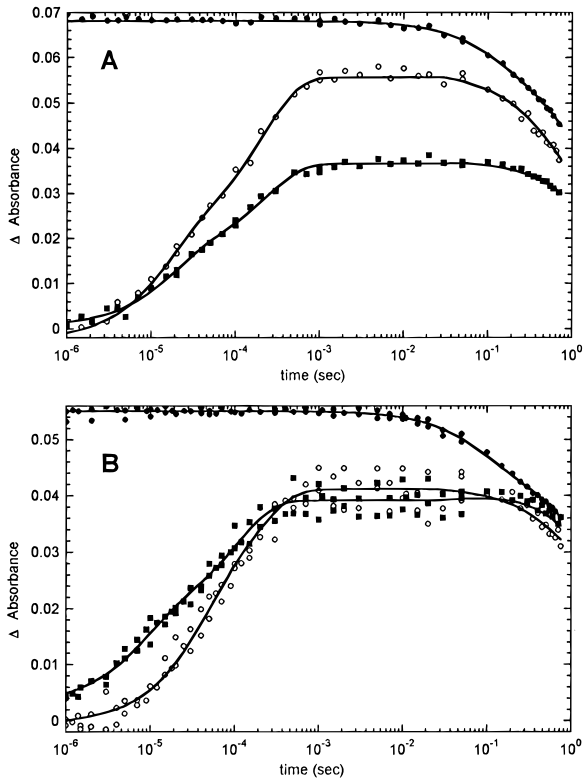

FIGURE 5: Time courses for absorbance changes associated with the $Q_A^-Q_B \rightarrow Q_AQ_B^-$ electron transfers for reaction centers in 50% ethylene glycol at room temperature. Parts A and B show data for reconstituted and native Q_B reaction centers, respectively. The absorbance data are marked as described in previous figures; 757 and 770 nm absorbance changes are indicated by filled squares and open circles, respectively, and P^+ extents are marked by filled circles. The 770 nm absorption changes are plotted with an inverted sign, and the amplitudes of the 757 and 770 nm absorbance changes are normalized to ΔA(865 nm, 0 μs) = 1. The extents of P^+ were scaled to fit into the figure. The solid lines are fits described in the text.

kinetics for reconstituted Q_B reaction centers are shown in part A. The absorbance changes at 757 nm were fit with a biexponential rise, having lifetimes of 18 ± 4 and 235 ± 45 μs, with relative amplitudes of 0.47 and 0.53, respectively. The absorbance changes at 770 nm were fit with lifetimes of 17 ± 8 and 231 ± 80 μs, with relative amplitudes of 0.45 and 0.55, respectively. The kinetics of the absorption change at 770 nm are seen to approximately parallel those measured at 757 nm with reconstituted Q_B reaction centers at room temperature both in the presence and in the absence of 50% ethylene glycol. The fits using biexponential kinetics suggest that the primary effect of the addition of 50% ethylene glycol to reconstituted reaction centers is on the fast component. The rise time of the fast component is seen to decrease from 37 to 18 μs, and the relative amplitude increases from 0.23 to 0.47. A summary of the 757 nm kinetics is given in Table 1.

The effect of ethylene glycol was found to be more evident with native Q_B reaction centers. Figure 5B shows 757 and 770 nm kinetics for native Q_B reaction centers in 50% ethylene glycol at room temperature. The kinetics at 757 nm were fit with rise times of 9 ± 4 and 107 ± 45 μs and relative amplitudes of 0.47 and 0.53, respectively. The addition of 50% ethylene glycol is seen to approximately double the amplitude of the fast kinetic component in the 757 nm absorption transients and to approximately halve the rise time in both native and reconstituted Q_B reaction centers. These results are summarized in Table 1.

Table 1: Summary of Biexponential Amplitude and Lifetime Parameters Used To Fit 757 nm Absorbance Changes in Reaction Center Preparations

	biexponential fits to 757 nm absorbance changes			
RC/conditions	τ_1 (μs)	A_1	τ_2 (μs)	A_2
reconstituted Q_B	37 ± 17	0.23	233 ± 50	0.77
native Q_B	25 ± 8	0.25	208 ± 40	0.75
reconstituted Q_B/50% ethylene glycol	18 ± 4	0.47	235 ± 45	0.53
native Q_B/50% ethylene glycol	9 ± 4	0.47	107 ± 37	0.53

In contrast to the approximately equivalent kinetics seen at the peak and trough of the Bph band shift with reconstituted reaction centers, the addition of ethylene glycol clearly separated the kinetics measured at 757 and 770 nm with native Q_B reaction centers. The kinetics at 770 nm were fit with rise times of 37 ± 20 and 200 ± 100 μs and relative amplitudes of 0.54 and 0.46, respectively. A slight disparity was noted between the kinetics at 757 and 770 nm for native Q_B reaction centers in the absence of ethylene glycol. This wavelength-dependent variation in kinetics was accentuated by the addition of ethylene glycol and can be more clearly illustrated at lower temperatures.

Temperature Dependence of Electrochromism Associated with the $Q_A^-Q_B \rightarrow Q_AQ_B^-$ Reaction. Transient spectra, $(P^+Q^-)_t$, measured with native Q_B reaction centers in 50% ethylene glycol at −22 °C are shown in Figure 6A, measured with 0 μs and 50 ms time delays. At this temperature, the absorption bands have narrowed somewhat, and the absorption peak for P has shifted from 865 nm at room temperature to 874 nm. Compared to room-temperature transient spectra, the peak and trough positions of the Bph band shifts are more clearly resolved, and the Bph shifts are seen to be different in the $P^+Q_A^-$ and $P^+Q_B^-$ states. These spectra more clearly indicate that the Q_A and Q_B anions primarily perturb different Bph transitions and that the effect of the Q_B anion is weaker than that of the Q_A anion.

Difference spectra for native Q_B reaction centers in 50% ethylene glycol at −22 °C are shown in Figure 6B, calculated from $(P^+Q^-)_t$ spectra with time delays of 10 μs, 1 ms, and 50 ms. Spectra recorded at early time delays differ from later spectra by showing a strong asymmetry of the Bph band shift and by the absence of absorption changes in the Bchl region. For example, the 10 μs spectrum shown in Figure 6B exhibits an absorbance increase with a peak at 757 nm without an accompanying absorption trough near 770 nm or absorption changes near 800 nm. The absorption decreases at 770 nm and absorption changes in the Bchl region are seen to develop in later spectra, illustrated by the 1 and 50 ms spectra in Figure 6B. The extent of the asymmetry of the Bph band shift varied in different native Q_B preparations. The cause of this variation is not known. The isosbestic point for the difference spectra in Figure 6B occurs above the zero crossing points. This raises the possibility that an offsetting absorbance increase obscured the expected bleaching in the 770 nm region. Broad absorbance changes in this region were seen in reaction centers containing the inhibitor stigmatellin, as described below. These spectra suggest that the wavelength region near 770 nm is likely to be congested

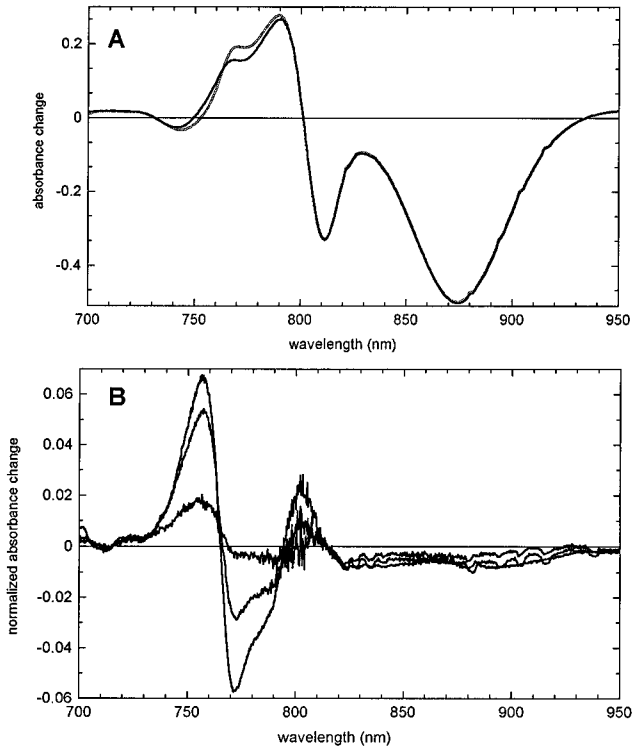

FIGURE 6: (A) transient $(P^+Q^-)_t$ spectra for native Q_B reaction centers in 50% ethylene glycol at −20 °C. The dotted and solid lines mark spectra measured 0 μs and 50 ms following 614 nm laser excitation. The reaction centers were suspended in 50% ethylene glycol, 0.8% OG, and 10 mM Tris at pH 7.8. Part B shows $Q^-(t) - Q_A^-(0\ \mu s)$ difference spectra, calculated from transient P^+Q^- spectra described in part A and recorded with delay times of 10 μs, 1 ms, and 50 ms.

with overlapping absorption changes from both Bchl and Bph cofactors, possibly including changes in transitions arising from optical couplings between cofactors, while absorbance changes near 757 nm are most likely to reflect the electrochromic response primarily of the Bph.

The kinetics of the absorption changes at 757, 772, and 803 nm are shown in Figure 7. The 803 nm curve tracks absorbance changes of the Bchl cofactors, measured at the absorbance peak in the difference spectra. Obvious differences are seen in the rise times of the absorbance changes at each of these three wavelengths. This figure illustrates that a strong wavelength dependency develops in the kinetics at low temperatures. In particular, it is important to note that the absorbance changes of the Bchl at 803 nm are not kinetically matched to those of the Bph. This indicates that the Bchl and Bph cofactors respond to different molecular events. As discussed below, we interpret the 757 nm change to reflect the $Q_A^-Q_B \rightarrow Q_AQ_B^-$ electron transfer event and the absorbance changes at 803 nm to reflect slower responses of the Bchl after the formation of the $P^+Q_B^-$ state.

Figure 7 also shows that the rise of the absorption change at 757 nm is broadly distributed in time at −22 °C. The absorbance change begins at 1 μs and continues to build in at 20 ms. An inflection in the 757 nm rise is seen near 10 μs, but this rise is too gradual to be fit as a single-exponential component. Unlike the room-temperature data, the 757 nm kinetics at this temperature cannot be fit as the sum of two exponential components. Fitting of the kinetic data at low temperatures requires a more dispersive kinetic model. Kinetic models of this sort (Frauenfelder & Wolynes, 1994;

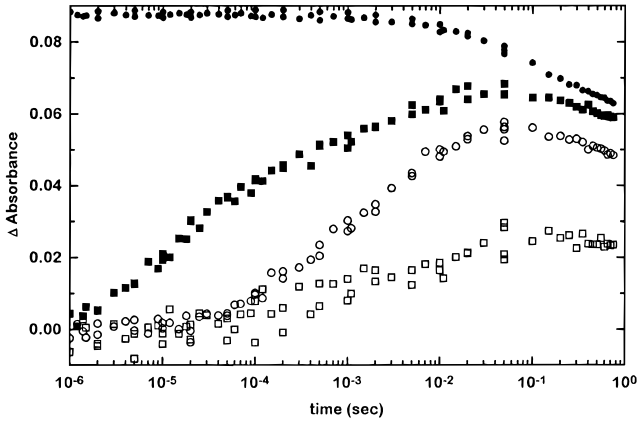

FIGURE 7: Time courses for absorbance changes associated with the $Q_A^-Q_B \rightarrow Q_AQ_B^-$ electron transfer in native Q_B reaction centers at −20 °C. Time courses are plotted for absorbance changes measured at 757 nm (filled squares), 770 nm (open circles), and 803 nm (open squares). The data were taken from spectra described in Figure 6. The 770 nm absorption changes are plotted with an inverted sign, and the amplitudes of the 757, 770, and 803 nm absorbance changes are normalized to $\Delta A(865\ nm, 0\ \mu s) = 1$. The filled circles mark the extent of P^+ measured by 865 nm bleaching and scaled to fit into the figure.

Hagen et al., 1995) imply that the reaction center exists in a distribution of slowly interconverting conformations that are distinguishable by differences in the rates of the absorbance changes associated with the $Q_A^-Q_B \rightarrow Q_AQ_B^-$ electron transfer. At lower temperatures the width of the distribution appears to increase, along with a decrease in the yield of the $P^+Q_B^-$ state. The loss of the yield of the $P^+Q_B^-$ state can be identified with the failure of the $Q_A^-Q_B \rightarrow Q_AQ_B^-$ electron transfer rates to compete with the $P^+Q_A^-$ back-reaction. This kinetic failure occurs at warmer temperatures in reconstituted Q_B reaction centers compared to native Q_B reaction centers.

Excitation Wavelength Dependence. All of the preceding data were collected using 614 nm laser excitation, which excites primarily the Q_x transition of P (Clayton et al., 1979; Rafferty & Clayton, 1979). We also collected a companion set of data using 532 nm excitation, which coincides with the Q_x peak of the Bph closest to Q_B. No significant differences were observed between these two sets of data at room temperature. Differences were observed at low temperatures. Figure 8 shows an example of this effect. The figure compares 757 nm absorption transients measured in the same native Q_B reaction center preparation at −22 °C using 532 and 614 nm excitations. In contrast to the kinetic behavior described in the previous paragraph, the initial absorbance rise at 757 nm builds in more steeply with 532 nm excitation and can be fit as a single-exponential component with a 10 ± 2 μs rise time. A second slower rise is also seen, but the rise of this component could not be fit as a single-exponential component at temperatures below −20 °C. The difference between the kinetics measured with 532 and 614 nm excitation appeared not to be trivially linked to differences in laser artifacts. Both laser light intensities were adjusted to give 60−80% saturation, and the experiments were performed using a flow cell that brought a new dark-adapted and temperature-equilibrated sample before laser flash excitation. These experiments suggest that the energy dissipated following absorption of the 532 nm photon narrows the distribution of reaction center configurations having fast kinetic rise times.

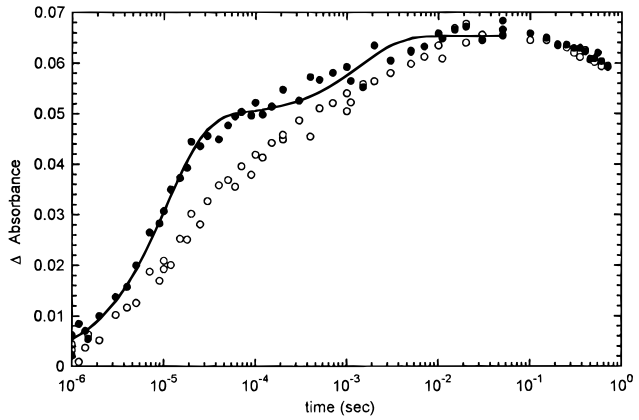

FIGURE 8: Comparison of time courses of 757 nm absorbance changes measured in native Q_B reaction centers at −20 °C using 532 and 614 nm excitation. The filled and open circles mark data recorded using 532 and 614 nm excitation, respectively. The line shapes of the $Q^-(t) - Q_A^-(0\ \mu s)$ difference spectra changed with laser excitation wavelength. At 757 nm, the amplitude of the absorbance change recorded with 532 nm excitation was larger than that seen with 614 nm excitation. For comparison of the kinetics of the 757 nm absorption changes, the data recorded with 532 nm excitation were scaled to match the extent of the absorption change using 614 nm excitation at 50 ms. The normalization constant was 0.625.

P^+Q^- charge recombination kinetics and $Q_A^-Q_B \rightarrow Q_AQ_B^-$ electron transfer kinetics have been observed to change upon cooling reaction centers to cryogenic temperatures under illumination (Kleinfeld et al., 1984b). The broadening of the kinetic distributions seen in this previous work has been attributed to freezing-in of conformational changes induced following generation of P^+Q^- charge-separated states. The effect described here is different. The narrowing of the kinetic distribution by 532 nm excitation is suggested to arise from energy dissipation before the P^+Q^- states develop.

Although in the kinetics of the 757 nm absorbance changes measured below −20 °C using 614 nm excitation do not follow simple, biexponential behavior, the inflections seen in these curves suggest that the reaction center distributions are centered around kinetically fast and slow configurations, analogous to the bimodal distributions seen at room temperature. The narrowing of the kinetic distribution of the fast component by 532 nm excitation allows the temperature-dependent behavior of this component to be more easily described. Figure 9 shows an Arrhenius plot of rate constants observed using 532 nm excitation. The slopes of the fitted lines yield activation energies of 4.5 and 11.0 kcal/mol with *y*-axis intercepts of 2×10^{-9} and 7×10^{-13} s^{-1} for the fast and slow components, respectively. The intercepts indicate that the slow component has a higher intrinsic probability for electron transfer. Significantly, this plot indicates that the relative incompetency of the slow component arises from a higher activation energy compared to that of the fast component and not from Arrhenius prefactors.

Electrochromism Resolved during the $P^+Q_A^-$ State. Absorption changes resolved during the lifetime of the $P^+Q_A^-$ state are shown in Figure 10. The difference spectra shown were recorded at room temperature with time delays of 10 μs, 1 ms, and 50 ms, using native Q_B reaction centers with 60 μM stigmatellin to replace Q_B. Parenthetically, we note that these experiments were tried using Q_B-depleted reaction centers (Okamura et al., 1975) and reaction centers with 400 μM *o*-phenanthroline. In both cases, 2−5% of Q_A appeared

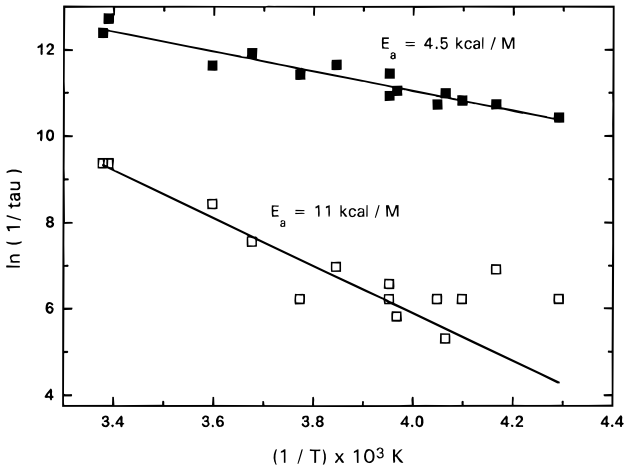

FIGURE 9: Arrhenius plots for the fast and slow kinetic components measured at 757 nm in native Q_B reaction centers using 532 nm excitation. The assay solution contained 50% ethylene glycol, 0.8% OG, and 10 mM Tris at pH 7.8.

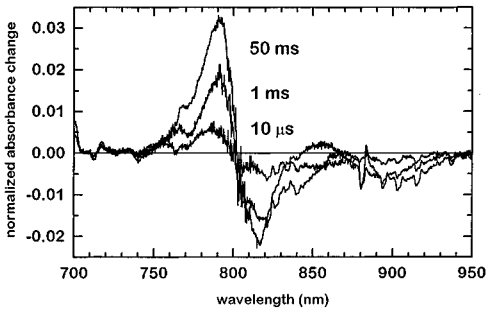

FIGURE 10: $Q^-(t) - Q_A^-(0\ \mu s)$ difference spectra for stigmatellin-inhibited, reconstituted Q_B reaction centers at room temperature. The spectra shown were calculated from $(P^+Q^-)_t$ spectra recorded with time delays of 10 μs, 1 ms, and 50 ms. The assay buffer contained 60 μM stigmatellin, 0.8% OG, and 10 mM Tris at pH 7.8.

to be displaced, as indicated by the presence of the triplet signal in the initial, 0 μs transient spectrum. This complication was minimized by using stigmatellin as a Q_B inhibitor.

The absorption changes observed during the lifetime of the $P^+Q_A^-$ state appear to involve exclusively the Bchl cofactors. At early times, illustrated by the 10 μs and 1 ms spectra in Figure 10, only small absorption changes are seen near 800 nm that are approaching the signal to noise limit in these experiments. At later times, a broad absorbance increase with a peak near 790 nm is seen to build in, illustrated by the 50 ms spectrum. Figure 11 shows a plot of the time course for the appearance of the 790 nm change, along with a plot of the absorbance changes at 757 nm. This time course shows that the rise time of the 790 nm change is comparable to the lifetime of $P^+Q_A^-$, preventing the full development of this feature. Similar results were obtained at −20 °C, and with reconstituted Q_B reaction centers.

It is important to note that the absorption changes observed during the lifetime of the $P^+Q_A^-$ differ markedly from those associated with the $Q_A^-Q_B \rightarrow Q_AQ_B^-$ electron transfer. Most significantly, there are only negligible absorption changes near 757 nm, which is the peak position for the Bph change during the $Q_A^-Q_B \rightarrow Q_AQ_B^-$ electron transfer. These results show that in this wavelength region P^+ and Q_A^- do not contribute to absorbance changes measured during the $Q_A^-Q_B \rightarrow Q_AQ_B^-$ electron transfer. Furthermore, the absorption changes characterized by the appearance of a 790 nm

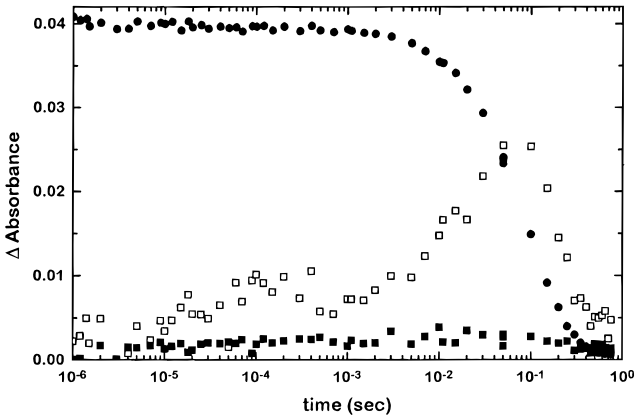

FIGURE 11: Time courses for light-induced absorbance changes in stigmatellin-inhibited, reconstituted Q_B reaction centers at room temperature. Time courses are plotted for absorbance changes measured at 757 nm (filled squares) and 790 nm (open squares). The data were taken from spectra described in Figure 10. The amplitudes of the 757 and 790 nm absorbance changes were normalized to ΔA(865 nm, 0 μs) = 1. The filled circles mark the extent of P^+ measured by 865 nm bleaching and scaled to fit into the figure.

absorption during the lifetime of the $P^+Q_A^-$ state occur after the $Q_A^-Q_B \rightarrow Q_AQ_B^-$ electron transfer would have finished in Q_B-containing, uninhibited reaction centers. Hence, we conclude that all of the absorption changes observed in Q_B-containing, uninhibited reaction centers are associated with the $Q_A^-Q_B \rightarrow Q_AQ_B^-$ electron transfer, and subsequent relaxation events, and are not influenced by time evolution in the P^+ or Q_A^- states.

DISCUSSION

Preparation Dependencies. Time-dependent electrochromic responses to $Q_A^-Q_B \rightarrow Q_AQ_B^-$ electron transfer were found to vary in different reaction center preparations. The kinetics of the absorption changes were consistently measured to be faster in native Q_B reaction centers than in reaction centers with reconstituted Q_B. Kinetics were found to be slower and more variable in preparations that used Triton rather than LDAO for reconstitution. Our measured lifetimes of 25 and 37 μs for the fast components of electron transfer in native and reconstituted Q_B reaction center preparations can be compared to a half-time of about 40 μs reported for this reaction in *Rb. sphaeroides* chromatophores (Crofts & Wraight, 1983). Our measurements of electrochromic events in *Rb. sphaeroides* chromatophores corroborate this approximate half-time but also indicate that the kinetics are multiphasic (D. M. Tiede and M. Batra, unpublished). This comparison suggests that the fast components may represent a configuration that is similar to that in the chromatophore membrane.

Preparation-dependent variations in the kinetics of the electrochromic response were more apparent for reaction centers in 50% ethylene glycol and at low temperatures. This effect can be attributed to a greater temperature sensitivity of the reaction rates in the reconstituted preparations that causes the $Q_A^-Q_B \rightarrow Q_AQ_B^-$ electron transfer rate to compete less effectively with the $P^+Q_A^-$ recombination in reconstituted Q_B preparations than for native Q_B reaction centers. The variation in the time-dependent electrochromic response to $Q_A^-Q_B \rightarrow Q_AQ_B^-$ electron transfer illustrates the sensitivity of the reaction center to preparative alteration. Reaction center crystal structures have shown considerable variability in quinone binding (Allen et al., 1988; Arnoux et al., 1989; El-Kabbani et al., 1991; Ermler et al., 1994). The following discussion emphasizes the importance of protein−quinone coupling as a variable but controlling feature of electron transfer.

Bph 757 nm Absorbance Change as an Indicator of the Q_B^- State. We have shown that the optical absorbance changes associated with the $Q_A^-Q_B \rightarrow Q_AQ_B^-$ electron transfer are complex, having heterogeneities with respect to time and wavelength. We find, however, that absorbance increases of the Bph near 757 nm are likely to reliably reflect the electron transfer event and formation of the Q_B^- state. This conclusion is supported by the specificity of this signal to the presence of the Q_B^- state. There are no absorbance changes of the Bph cofactors during the time evolution and decay of the $P^+Q_A^-$ state, and the kinetics of the 757 nm decay follow monotonically the $P^+Q_B^-$ recombination kinetics. This conclusion is also supported by the fast optical response at 757 nm. The rise of the absorbance peak at 757 nm is found to be the fastest optical response to the $Q_A^-Q_B \rightarrow Q_AQ_B^-$ electron transfer at all temperatures and solution conditions. We interpret the 757 nm optical response to reflect the electron transfer event. This conclusion supports earlier work (Vermeglio & Clayton, 1977) but is at odds with a recent suggestion that absorbance changes monitored at 760 nm lag behind electron transfer and respond mainly to proton transfer or to conformational changes in the protein (Hienerwadel et al., 1995). This latter suggestion arose from measurements of 760 nm absorption transients that showed no sub-millisecond kinetic components, in contrast to companion, time-resolved measurements of IR bands sensitive to the Q_B redox state (Hienerwadel et al., 1995). Our measurements contradict these findings. At 4 °C, we find the biphasic rise of the absorption changes at 757 nm to have time constants of approximately 10 and 200 μs for native Q_B reaction centers in 50% ethylene glycol and to have rise times of approximately 70 and 700 μs for reconstituted Q_B reaction centers without ethylene glycol.

One complication in the time-resolved Bph absorption changes is the pronounced difference in kinetics of the Bph absorbance peak at 757 nm and trough at 770 nm upon cooling. This effect is seen with both reconstituted and native Q_B reaction centers. At room temperature, kinetic differences at these wavelengths are not detected with reconstituted Q_B reaction centers but can be marginally resolved in native Q_B reaction centers. Time-resolved difference spectra recorded below −20 °C clearly show the absorbance increases at 757 nm to develop faster than the decreases at 770 nm. In many samples, the kinetic differences were sufficiently large that an absorption signal centered at 757 was recorded to appear first, followed by slower absorption decreases at 770 nm. Although electric field-induced changes in difference spectra can be expected to be a combination of zero-, first-, and second-derivative spectral shapes (Liptay, 1969), a kinetic separation is not expected. Complex electrochromism might be expected if heterogeneity in the reaction center sample caused the electric field perturbation by the $Q_A^-Q_B \rightarrow Q_AQ_B^-$ electron transfer to vary in different reaction center populations. A further complicating feature is the congestion of absorption bands in the 770 nm region. As discussed below, we have found that the Bchl and Bph absorptions respond to different

molecular events initiated by the $Q_A^-Q_B \rightarrow Q_AQ_B^-$ electron transfer. Different optical responses of the cofactors will greatly complicate kinetics in regions where the Bph and Bchl absorptions overlap. The blue edge of the Bph absorption is likely to be the least contaminated by optical transitions of other cofactors, and the 757 nm absorption change will most reliably detect the optical response of the Bph. Since our data show that the time evolution of P^+ and Q_A^- do not alter the Bph absorption, we conclude that electron transfer must be the initiating electrochromic event, and electron transfer must be reflected in the Bph 757 nm absorption change. Recent light-induced FTIR measurements show that the vibrational spectrum of the Bph next to the Q_A site is perturbed by the formation of the Q_A^- (Breton et al., 1996), although our results suggest that these perturbations are not sufficient to change the Q_y optical absorption.

Heterogeneous Rate of $Q_A^-Q_B \rightarrow Q_AQ_B^-$ Electron Transfer. The rate of the $Q_A^-Q_B \rightarrow Q_AQ_B^-$ electron transfer as measured by the peak 757 nm change was found to be heterogeneous and to be dependent upon the preparation, solution osmolarity, temperature, and excitation wavelength. Multiphasic $Q_A^-Q_B \rightarrow Q_AQ_B^-$ electron transfer kinetics have also been found from measurements of absorption transients of quinone anion absorption bands in the 400 nm region (Li et al., 1996). In this work, transient kinetics in the quinone anion bands were fit with three exponential components, having lifetimes of approximately 2, 80, and 200 μs in Q_B reconstituted reaction centers (Li et al., 1996; J. Li, D. Gilroy, and M. R. Gunner, personal communication). It is likely that our 37 μs component corresponds to the sum of the 2 and 80 μs components resolved in these experiments. The compatibility of the two sets of measurements is also indicated by the agreement in activation energies measured by Li et al. (1996) for the fast (2 and 80 μs) and slow (200 μs) components with those measured here. Biphasicity has also been observed in transient IR measurements, although on different time scales than those observed here (Hienerwadel et al., 1992, 1995). These data point toward the existence of two RC populations that differ in $Q_A^-Q_B \rightarrow Q_AQ_B^-$ electron transfer rate.

The temperature dependencies of the fast and slow $Q_A^-Q_B \rightarrow Q_AQ_B^-$ kinetic components, measured in 50% ethylene glycol and with 532 nm excitation, show that the most significant difference between the two populations lies with their activation energies for electron transfer rather than Arrhenius pre-exponential factors. Recent experiments by Graige et al. (1996) suggest that the electron transfer of the slow kinetic component is rate-limited by a protein conformational change. From this view, the kinetic heterogeneity would be attributed to arise from differences in the activation energies for protein reorganization in the different reaction center populations.

A surprising feature of our experiments was the excitation wavelength dependence of the $Q_A^-Q_B \rightarrow Q_AQ_B^-$ electron transfer kinetics at low temperatures. Unexpectedly, we find that distributed kinetics seen for the fast $Q_A^-Q_B \rightarrow Q_AQ_B^-$ reaction below −20 °C are removed by direct excitation of the Bph closest to Q_B with 532 nm light. Alteration of reaction kinetics by illumination while cooling has been linked to the trapping of reaction centers in altered conformations induced by the charge separation (Kleinfeld et al., 1984b). Subsequent excitation at low temperatures measures photochemistry for reaction centers with altered conformation. The effect reported here is different. Following excitation at low temperatures, a flow cell returned the sample to room temperature to allow for conformational equilibration in the dark. This system was used to avoid the buildup of altered conformations induced by photochemistry at low temperatures. A new, dark-adapted, thermally equilibrated sample was used for every measurement. There is a possibility that part of the effect might arise from multiple excitations of the reaction center by an intense laser pulse (Puchenkov et al., 1995). We attempted to equalize possible effects of laser artifacts by adjusting both 532 and 614 nm laser intensities to produce comparable extents of reaction center saturation (60−80%). There is a possibility that the kinetic discrepancies arise from impurities in the samples, but we find the same effect with purified reaction centers and with partially purified preparations. These experiments suggest that heat dissipated following excitation of the 532 nm-absorbing Bph, and not P, changes the distribution of conformational states, presumably in the vicinity of the Bph, and alters the $Q_A^-Q_B \rightarrow Q_AQ_B^-$ kinetics.

With 614 nm excitation, distributed kinetics are seen for both the fast and slow reaction center configurations below −20 °C. Inflections in the transient 757 nm data appear to track the biphasic rate constants observed with 532 nm excitation. This suggests that kinetics observed with 614 nm excitation are distributed around fast and slow reaction center configurations. The appearance of distributed kinetics at low temperatures is characteristic of freezing-in of conformational substates. These results suggest that a rapid interconversion of substates compared to electron transfer is a critical feature of the $Q_A^-Q_B \rightarrow Q_AQ_B^-$ reaction at room temperature. This characterization is compatible with the proposal that conformational changes limit the reaction rate for the slow component at room temperature (Brzezinski et al., 1992; Graige et al., 1996). Similar thermal averaging of conformational substates has been seen for reaction dynamics in other proteins (Frauenfelder & Wolynes, 1994; Hagen et al., 1995).

Kinetic heterogeneity also appears to be a general feature of $P + Q^-$ recombination reactions (Baciou & Sebban, 1995; Parot et al., 1987; Sebban & Wraight, 1989). Recent FTIR measurements have found evidence for heterogeneous Q_B binding, with 25% of the reaction centers exhibiting weak binding interactions between the protein and quinone carbonyls and 75% exhibiting stronger interactions (Brudler et al., 1995). These values are remarkably similar to the relative amplitudes of the fast and slow kinetic components determined here for both native and reconstituted Q_B reaction centers at room temperature.

The kinetic heterogeneity induced by freezing reaction centers in the light has also been well-studied. Analysis of electron spin polarization associated with the $P^+Q_A^-$ radical pair in samples that were frozen in the light and dark demonstrated that light-induced alteration in recombination kinetics occurs without modification of the geometry or distance relationship between the P^+ and Q_A^- radicals (van den Brink et al., 1994). This lack of correlation between changes in kinetic heterogeneity and the relative structure of the $P^+Q_A^-$ radical pair led to the conclusion that the light-induced alteration of recombination kinetics must be due to heterogeneities induced in the distribution of free energies for the $P^+Q_A^-$ states (van den Brink et al., 1994). Similarly, a study of the electric field dependence of $P^+Q_A^-$ recombi-

nation rates led to the conclusion that kinetic heterogeneity arises from differences in solvation energies rather than donor/acceptor structure (Franzen et al., 1990). Our findings that the fast and slow reaction center populations for $Q_A^-Q_B \rightarrow Q_AQ_B^-$ electron transfer differ most significantly in their Arrhenius activation energies for electron transfer rather than Arrhenius prefactors are compatible with these conclusions.

Decoupling of Bph and Bchl Absorption Changes. The results presented here show that the optical response of the Bchl and Bph cofactors to $Q_A^-Q_B \rightarrow Q_AQ_B^-$ electron transfer are not kinetically coupled. Particularly at −20 °C, the rise time of the Bchl change was seen to occur on the 1−100 ms time scale, while the Bph changes were distributed from 1 μs to 20 ms. The decoupling of Bph and Bchl absorption changes were seen in both native and reconstituted Q_B preparations, and with 614 and 532 nm excitations. These results demonstrate that Bchl responds to different, slower molecular events than Bph. As discussed below, the current experiments have not resolved separately the electrochromic events due to electron and proton movements. The observation that the absorption changes in the Bchl region during the $P^+Q_A^-Q_B \rightarrow P^+Q_AQ_B^-$ electron transfer are different from those measured during the lifetime of the $P^+Q_A^-$ state in stigmatellin-inhibited reaction centers also argues that Bchl is not responding to time evolution in the P^+ state. We suggest that Bchl absorption changes reflect delocalized conformation changes or slower relaxation events in response to the formation of the quinone anion states. Conformational changes in the reaction center have been suggested from measurements of capacitative charge movement with reaction centers imbedded in supported planar bilayers (Brzezinski et al., 1992) and transient IR measurements (Hienerwadel et al., 1992, 1995). In addition, trypsin lysis of reaction centers suggests that charge separation is accompanied by protein rearrangements that make the protein more accessible to trypsin degradation (Smirnova et al., 1995).

Proton Uptake Events. In the present analysis of $Q^-(t) - Q_A^-(0\ \mu s)$ difference spectra, electrochromism from proton and electron movements are not resolved because these spectra represent double-difference spectra, derived from the $(P^+Q^-)_t - n_t(P^+Q_A^-)_{0\ \mu s}$ difference. Hence, the transient spectra reflect the recovery both of the bacteriopheophytin absorption following Q_A^- oxidation and of the bacteriopheophytin red shift associated with the formation of Q_B^-. The extent of the bacteriopheophytin band shift associated with Q_B^- will be modulated by proton uptake and other relaxation events. The transient kinetics, particularly on the red edge of the bacteriopheophytin band, respond to a mixture of electron and proton transfer events. Time-dependent electrochromism associated with proton uptake and electron transfer can be resolved by recording time evolution of PQ^- spectra and deconvoluting bacteriopheophytin absorption shifts as a function of time. These analyses will be described in a subsequent publication.

REFERENCES

Allen, J. P., Feher, G., Yeates, T. O., Komiya, H., & Rees, D. C. (1988) *Proc. Natl. Acad. Sci. U.S.A. 85*, 8487−8491.

Arnoux, B., Ducruix, A., Reiss-Husson, F., Lutz, M., Norris, J., Schiffer, M., & Chang, C.-H. (1989) *FEBS Lett. 258*, 47−50.

Baciou, L., & Sebban, P. (1995) *Photochem. Photobiol. 62*, 271−278.

Bellissent-Funel, M.-C., Lal, J., Bradley, K. F., & Chen, S. H. (1993) *Biophys. J. 64*, 1542−1549.

Beroza, P., Fredkin, D. R., Okamura, M. Y., & Feher, G. (1991) *Proc. Natl. Acad. Sci. U.S.A. 88*, 5804−5808.

Beroza, P., Fredkin, D. R., Okamura, M. Y., & Feher, G. (1995) *Biophys. J. 68*, 2233−2250.

Breton, J., Nabedryk, E., Allen, J. P., & Williams, J. C. (1996) *Biophys. J. 40*, A355.

Brudler, R., de Groot, H. J. M., van Liemt, W. B. S., Gast, P., Hoff, A. J., Lugtenburg, J., & Gerwert, K. (1995) *FEBS Lett. 370*, 88−92.

Brzezinski, P., Okamura, M. Y., & Feher, G. (1992) in *The Photosynthetic Bacterial Reaction Center II* (Breton, J., & Vermeglio, A., Eds.) pp 321−330, Plenum Press, New York.

Bylina, E. J., Kirmaier, C. K., McDowell, L., Holten, D., & Youvan, D. C. (1988) *Nature 336*, 182−184.

Carithers, R. P., & Parson, W. W. (1975) *Biochim. Biophys. Acta 387*, 194−211.

Clayton, R. K., Rafferty, C. N., & Vermeglio, A. (1979) *Biochim. Biophys. Acta 546*, 58−68.

Colombo, M. F., Rau, D. C., & Parsegian, V. A. (1992) *Science 256*, 655−659.

Crofts, A. R., & Wraight, C. A. (1983) *Biochim. Biophys. Acta 726*, 149−185.

Demas, J. N. (1983) *Excited state lifetime measurements*, Academic Press, New York.

El-Kabbani, O., Chang, C.-H., Tiede, D. M., Norris, J., & Schiffer, M. (1991) *Biochemistry 30*, 5361−5369.

Ermler, U., Fritzsch, G., Buchanan, S. K., & Michel, H. (1994) *Structure 2*, 925−936.

Feher, G., Allen, J. P., Okamura, M. Y., & Rees, D. C. (1989) *Nature 339*, 111−116.

Franzen, S., Goldstein, R. F., & Boxer, S. G. (1990) *J. Phys. Chem. 94*, 5135−5149.

Frauenfelder, H., & Wolynes, P. (1994) *Phys. Today 47*, 58.

Graige, M. S., Feher, G., & Okamura, M. Y. (1996) *Biophys. J. 70*, A10.

Gunner, M. R. (1991) *Curr. Top. Bioenerg. 16*, 319−367.

Gunner, M. R., & Honig, B. (1991) *Proc. Natl. Acad. Sci. U.S.A. 88*, 9151−9155.

Hagen, S. J., Hofrichter, J., & Eaton, W. A. (1995) *Science 269*, 959−962.

Hanson, L. K., Fajer, J., Thompson, M. A., & Zerner, M. C. (1987) *J. Am. Chem. Soc. 109*, 4728.

Hienerwadel, R., Thibodeau, D., Lenz, F., Nabedryk, E., Breton, J., Kreutz, W., & Mantele, W. (1992) *Biochemistry 31*, 5799−5808.

Hienerwadel, R., Grzybek, S., Fogel, C., Kreutz, W., Okamura, M. Y., Paddock, M. L., Breton, J., Nabedryk, E., & Mantele, W. (1995) *Biochemistry 34*, 2832−2843.

Kleinfeld, D., Okamura, M. Y., & Feher, G. (1984a) *Biochim. Biophys. Acta 766*, 126−140.

Kleinfeld, D., Okamura, M. Y., & Feher, G. (1984b) *Biochemistry. 23*, 5780−5786.

Krishtalik, L. I. (1995) *Biochim. Biophys. Acta 1228*, 58−66.

Krishtalik, L. I. (1996) *Biochim. Biophys. Acta* (in press).

Larson, J. W., & Wraight, C. A. (1995) *Photosynth. Res.* (Suppl. 1), 65.

Leibl, W., & Breton, J. (1991) *Biochemistry 30*, 9634−9642.

Li, J., Gilroy, D., & Gunner, M. (1995) *Biophys. J. 70*, A10.

Liptay, W. (1969) *Angew. Chem., Int. Ed. Engl. 8*, 177−188.

Mancino, L. J., Dean, D. P., & Blankenship, R. E. (1984) *Biochim. Biophys. Acta 764*, 46−54.

Marcus, R. A. (1964) *Annu. Rev. Phys. Chem. 15*, 155−196.

Marcus, R. A., & Sutin, N. (1985) *Biochim. Biophys. Acta 811*, 265−322.

Maroti, P., & Wraight, C. A. (1988) *Biochim. Biophys. Acta 934*, 314−328.

McPherson, P. H., Okamura, M. Y., & Feher, G. (1988) *Biochim. Biophys. Acta 934*, 348−368.

Okamura, M. Y., & Feher, G. (1992) *Annu. Rev. Biochem. 61*, 861−896.

Okamura, M. Y., Isaacson, R. A., & Feher, G. (1975) *Proc. Natl. Acad. Sci. U.S.A. 72*, 3491−3495.

Paddock, M. L., Feher, G., & Okamura, M. Y. (1991) *Photosynth. Res. 27*, 109−199.

Parot, P., Thiery, J., & Vermeglio, A. (1987) *Biochim. Biophys. Acta 893*, 534−543.

Parsegian, V. A., Rand, R. P., Fuller, N. L., & Rau, D. C. (1986) *Methods Enzymol. 127*, 400.
Press, W. H., Teukolsky, S. A., Vetterling, W. T., & Flannery, B. P. (1992) *Numerical recipes in C: the art of scientific computing*, Cambridge University Press, Cambridge.
Puchenkov, O. A., Kopf, Z., & Malkin, S. (1995) *Biochim. Biophys. Acta 1231*, 197−212.
Rafferty, C. N., & Clayton, R. K. (1979) *Biochim. Biophys. Acta 546*, 189−206.
Rand, R. P. (1992) *Science 256*, 618.
Sebban, P., & Wraight, C. A. (1989) *Biochim. Biophys. Acta 974*, 54−65.
Shinkarev, V. P., & Wraight, C. A. (1993) in *The photosynthetic reaction center* (Deisenhofer, H., & Norris, J. R., Eds.) pp 193−255, Academic Press, New York.
Shopes, R. J., & Wraight, C. A. (1985) *Biochim. Biophys. Acta 806*, 348−356.
Smirnova, I. A., Blomberg, A., Andreasson, L.-E., & Brzezinski, P. (1995) *Photosynth. Res.* (Suppl. 1), 69.
Steffen, M. A., Lao, K., & Boxer, S. G. (1994) *Science 264*, 810−816.
Takahashi, E., & Wraight, C. A. (1992) *Biochemistry 31*, 855−866.
Tang, J., & Norris, J. R. (1988) *Nucl. Instrum. Methods Phys. Res. A273*, 388−342.
Tiede, D. M., & Hanson, D. K. (1992) in *The Photosynthetic Bacterial Reaction Center II* (Breton, J., & Vermeglio, A., Eds.) pp 341−350, Academic Press, New York.
van den Brink, J. S., Hulsebosch, R. J., Gast, P., Hore, P. J., & Hoff, A. J. (1994) *Biochemistry 33*, 13668−13677.
Vermeglio, A., & Clayton, R. K. (1977) *Biochim. Biophys. Acta 461*, 159−165.
Wraight, C. A. (1979) *Biochim. Biophys. Acta 548*, 309−327.

BI9605907